Dynamic Model of a Novel Planar Cable Driven Parallel Robot with a Single Cable Loop

Antonio Gonzalez-Rodríguez , Andrea Martín-Parra * , Sergio Juárez-Pérez , David Rodríguez-Rosa , Francisco Moya-Fernández , Fernando J. Castillo-García , Jesús Rosado

Posted Date: 11 April 2023

doi: 10.20944/preprints202304.0184.v1

Keywords: Cable-Driven Parallel Manipulator; Dynamic model; Workspace

Article

Dynamic Model of a Novel Planar Cable Driven Parallel Robot with a Single Cable Loop

Antonio González-Rodríguez [1,†], Andrea Martín-Parra [1,*,†], Sergio Juárez-Pérez [1,†], David Rodríguez Rosa [1,†], Francisco Moya-Fernández [1,†] Fernando J. Castillo-García [1,†] and Jesús Rosado-Linares [1,†]

[1] School of Industrial and Aerospace Engineering, University of Castilla-La Mancha, Av. Carlos III, 45071 Toledo, Spain; antonio.gonzalez@uclm.es (A.G.-R.); sergio.juarez@uclm.es (S.J.-P.); david.rrosa@uclm.es (D.R.R.); francisco.moya@uclm.es (F.M.-F.); fernando.castillo@uclm.es (F.J.C.-G.); jesus.rosado@uclm.es (J.R.-L.)

* Correspondence: andrea.martin@uclm.es

† These authors contributed equally to this work.

Abstract: Cable-Driven Parallel Robots (CDPRs) are a special kind of parallel manipulator which use cables to control the position and orientation of the mobile platform or end-effector. The usage of cables instead of rigid links offer some advantages over their conventional rigid counterparts. As cables can only pull, but not push, the number of cables (n) required to command the end-effector is always $n+1$. This configuration is known as fully-constrained and it is the most extended configuration for CDPRs. Although CDPRs have many advantages, such as their ability to cover large working areas, one of their main problems is that their working area (workspace) is limited in comparison to its frame area (planar case), or frame volume (spatial case), due to the minimum and maximum allowed tensions. Depending of these tensions values the workspace can be notoriously decreased. In order to tackle this problem, lots of works focus on solving kinematics or dynamics problems for cable sagging, i.e., they take into account sagging when modelling the robot kinematic and include these poses inside the usable robot workspace. Taking into account phenomenons like this increases the mathematical complexity of the problem, and much more complex techniques are required. On the other hand, the lack of workspace problem can be tackled by adding active or passive elements to the robot design. In this sense, this paper proposes two mechanical modifications: to add passive carriages to the robot frame and to use a single cable loop to command the end-effector position and orientation. This work presents the kinematic, static and dynamic models of the novel design and shows the gain of workspace for a planar case while taking into account different parameters of the robot.

Keywords: cable-driven parallel manipulator; dynamic model; workspace

1. Introduction

Cable-Driven Parallel Robots (CDPRs) are a kind of parallel manipulators in which cables replace rigid links. Alternatively, a CDPR can be viewed as a dexterous lifting machine which uses several cables to avoid, at least partially, a sway of the payload. CDPRs generally consist of a supporting structure, winches winding up the cables, and a payload (mobile platform) where the cables are attached [1]. The moving platform or end-effector is connected to a number of winches by means of cables. The cables are stored on the winch drums and may be routed to the end-effector by means of one or several pulleys. They can be attached directly to the end-effector or connected to it by means of universal joints. The end-effector position and orientation, hereafter pose, can be controlled by varying the length of the cables [2]. In addition, a motion of the mobile platform can also induced by varying the cable forces, i.e., the actuated winches that roll the cables in drums, can control the end-effector pose by adjusting cable lengths or tensions [1]. The pros and cons of a CDPR usually depend on a particular application context but some general advantages of this kind of manipulators are simple

structure, high precision, small volume of the actuator, small inertia force, and low manufacturing cost as cables are easy to wind, and the robot actuators only need to support the end-effector and cables payload [3–5]. Moreover, distinctive advantages of CDPRs are scalability, a potentially very large workspace and the ability to handle very heavy payloads [1]. Due to the advantages of CDPRs, research on CDPRs has gained wide attention and is highly motivated by the modern engineering demand for large load capacity and workspace. CDPRs have been increasingly and widely applied in relevant tasks, such as construction, rescue systems, rehabilitation, and even three-dimensional printing [6].

On the other hand, one of the main problems of CDPRs is maintaining cable tensions within acceptable limits. Cables can only pull, but not exert compression forces so tensions must remain positive in order to solve the equilbrium equation [7]. In fact, cable tensions must remain above a certain tension level (lower limit) to avoid cable sagging. The sagging in cables yields to problems while coiling the cables and/or positioning errors if the kinematic model, as it is commonly done, does not consider this effect. The upper tension limit is mostly related with the maximum torque that can be exerted by the actuators.

CDPRs can be classified according to their structure, the number of degrees-of-freedom (DOFs), m, and the number of cables, n, where $r = m - n$ is the number of redundant cables or the number of degrees of redundancy. According to this, CDPRs can be classified as [8]:

- $r < 0, m \leq 6$ incompletely restrained positioning mechanism or underconstrained CDPR. These type of CDPR can only reach equilibrium with gravity or a given force, and often cannot work with arbitrary external wrenches.
- $r = 0$ kinematically fully constrained CDPR. The robot is completely limited in terms of kinematics, but the equilibrium equation still depends on gravity or other forces. That is to say, the robot can only work with a specific set of forces.
- $r = 1$ completely restrained positioning mechanisms or fully constrained CDPR. The end-effector poses can be determined entirely through the cables. The limits of the end-effector movements and the wrenches acting on the end-effector depend on the cable tension limits.
- $r > 1$ redundantly restrained positioning mechanisms or over constrained CDPR. The robot is constrained redundancy and wrenches must be distributed by cables. The number of kinematic constraints is greater than the number of DOFs so the static equilibrium of CDPR can have many solutions.

Other classification based on the direction of gravity towards the end-effector classifies CDPRs as suspended when cables are mounted in the direction of gravity. This configuration relies on the influence of gravity on the end-effector to achieve the equilibrium state [9]. Depending on the design configuration, some CDPRs operate only in the suspended state, some CDPRs can operate in the fully restrained state, or may operate both in the fully restrained state and in the suspended state [3].

In the case of conventional CDPRs (fully constrained CDPRs) the limitations in cable tensions yield to a significant reduction of the robot's wrench-feasible workspace (WFW) [10] compared to its frame area. The upper tension limit reduces the upper part of the workspace, while the lower tension limit is related to the loss of space on both sides. The only possible way to overcome this loss of working space, without modifying the robot design, is to enlarge the tensions limits. Expanding the tension limits implies increasing the torque capacity or considering the sagging effect in the kinematic model, respectively. Many authors have tackled this problem by adding active elements to the design, that in fact, improves the robot overall dexterity. A few examples of reconfigurable cable positioning taking into account the end-effector trajectory, or moving the cables anchor points so collisions are avoided can be found in works such as [11–14]. Other authors propose modifying the attachment of the anchor points in the end-effector so collision with elements is avoided while reducing the end-effector manoeuvring [15,16]. All these solutions have the drawback of adding more actuators to the design, whereas previous works such as [17,18] proves that there is no need to add active

 doi:10.20944/preprints202304.0184.v1

elements to the design. Instead, it was shown that adding passive elements, such as moving carriages, to the design immensely increases the WFW of the robot. Taking into account the kinematic and static models analysis presented in [18], it is remarkable how the mechanical modification of adding passive carriages to the design increases the robot WFW. These carriages can move freely along linear guides in the robot frame. Moreover, passive carriages have pulleys that redirect the cable towards the end-effector decreasing the variation in cable direction during the end-effector travelling. In this way, the required cable tension is lower, achieving reasonable tension limits and a much larger WFW. Apart from comparing the WFW of the new design with a conventional CDPR, [18] also develops an analysis on the implications of the robot geometry in the achievable WFW, i.e., a parametric analysis. The main disadvantage of this new design is the end-effector loss of stiffness along the x-axis. In [18] a stiffness analysis was introduced to further propose a solution.

In order to tackle the stiffness related problem when adding passive carriages to a CDPR this paper proposes another mechanical modification: using a single cable loop to command the end-effector pose. With this novel design not only there is a WFW enlargement and a much lower required motorization, but also the stiffness of the proposed CDPR is constant over the entire WFW. Together with the mechanical concept presentation, this paper introduces the mathematical foundations including kinetostatic analysis. Then, the WFW of the robot is analysed and compared to that of a conventional CDPR, adding a stiffness synthesis within the WFW of the robot. Finally, the control strategy is proposed and simulated and experimental results are presented.

The paper is organised as follows. Section 2 describes the overall proposal and nomenclature, highlighting the advantages in terms of feasible workspace. Section 3 introduces the mathematical foundations of the new CDPR design, including the kinematic, static and dynamic models. Section 4 describes the experimental platform used to validate the model, including the computer vision system used to track the end-effector. Section 5 describes the experiments carried out to validate the model. Section 6 describes a simple kinematic control scheme intended to show the controlability of the system. Finally Section 7 draws some conclusions and proposes lines for future work.

2. System description

2.1. Workspace limitations

To illustrate the workspace limitations of CDPR, let's assume a fully-constrained planar scheme as in Figure 1 where:

- H and W are the height and width of the frame, respectively.
- h and w are the height and width of the end-effector, respectively.
- T_i for $i = 1, ..., 4$ the tension of the cables.
- τ_i for $i = 1, ..., 4$ the torques exerted by each motor.
- r the effective radius of the drums.
- $[x_e, y_e, \delta_e]$ the coordinates of the end-effector.

Preprints (www.preprints.org) | NOT PEER-REVIEWED | Posted: 11 April 2023 doi:10.20944/preprints202304.0184.v1

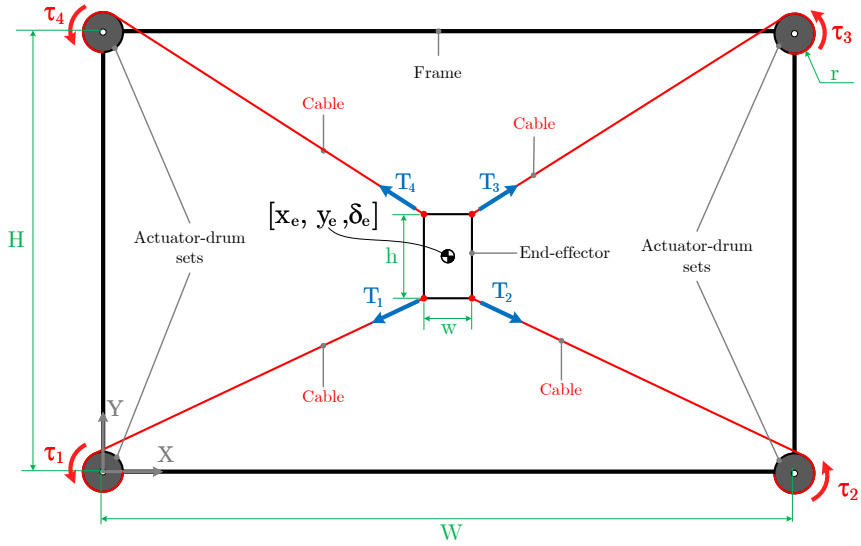

Figure 1. Conventional planar CDPR

Assuming that no sagging cables are allowed (e.g. [19], the static workspace of the robot can be determined by imposing end-effector poses within the frame and checking if the force/torque equilibrium can be achieved for these poses. The main parameters affecting the workspace are the dimensional parameters of the robot (W,H, w, h and r), the end-effector mass matrix, M, and the allowable tension limit values: T_{min} and T_{max} [20]. The minimum tension value, T_{min}, must be set to avoid sagging cables and low stiffness values. The maximum tension value, T_{max}, is determined by the maximum holding torque of the motors and by the breaking strength of the cables [21].

Figure 2 shows the static workspace of the robot scheme of Figure 1 with the parameters of the prototype presented in the experimental results section: $W = 2.224$ m, $H = 1.112$ m, $w = 0.281$ m, $h = 0.287$ mm, $m = 2$ kg and no rotation of the end-effector $\delta = 0°$. Figure 2 illustrates that for a minimum tension value, $T_{min} = 2.5$ N, the static workspace is only the 27.56% of the frame area. The static workspace is reduced when the allowed minimum tension increases and for $T_{min} = 7.0$ N only the 10.53% of the frame area is accessible to the end-effector.

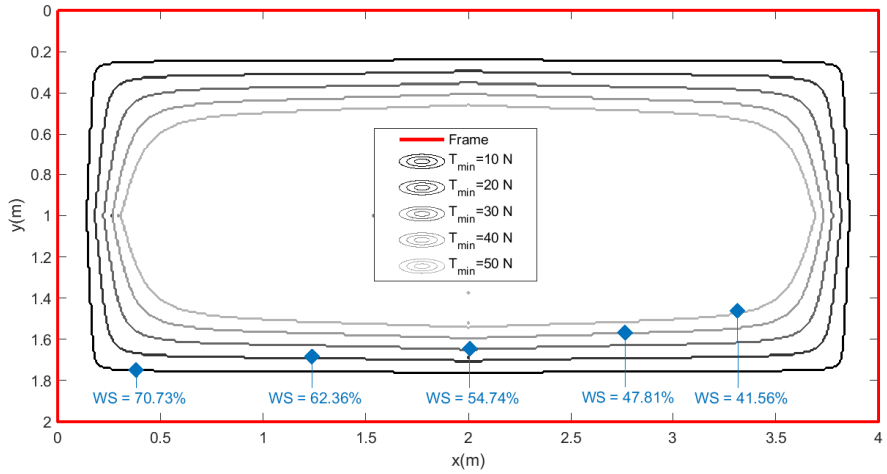

Figure 2. Workspace of the conventional planar CDPR

Preprints (www.preprints.org) | NOT PEER-REVIEWED | Posted: 11 April 2023 doi:10.20944/preprints202304.0184.v1

2.2. Novel single cable loop CDPR

As mentioned in Section 1, some of the main drawbacks of CDPR are: a) the limited workspace inside of the frame [20]; b) the lack of the robot dexterity when the end-effector is placed near the boundaries of the feasible workspace [22].

For solving these two problems, this paper proposes the single cable loop cable-driven parallel robot (sCDPR) scheme shown in Figure 3. The proposal is based on the addition of two passive carriage-linear guide sets in the upper and lower part of the frame. Through a set of driven pulleys a single cable loop can be designed and its length will remain constant for any pose of the end-effector (assuming negligible in this first step the length variation of the cable due to its elasticity). Two actuators, placed at the lower corners of the frame, provide the movement capability of the end-effector through driven pulleys.

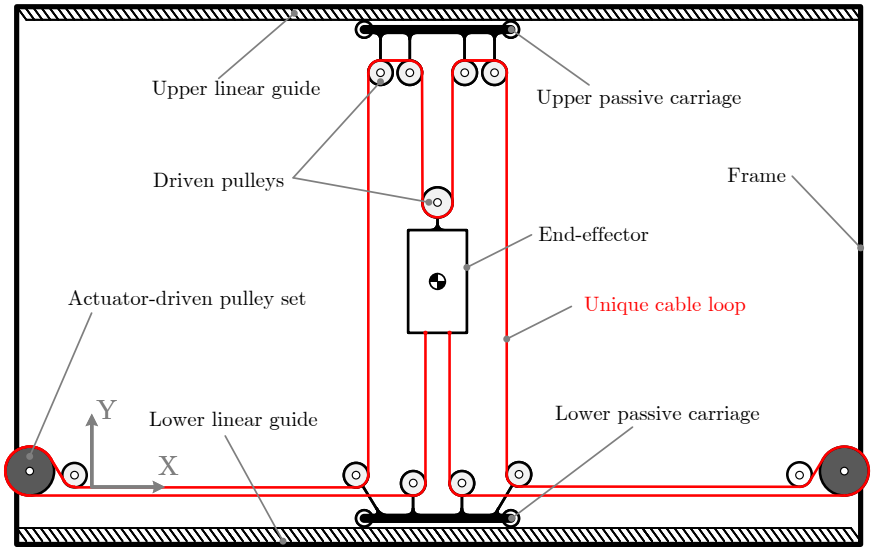

Figure 3. Single cable loop planar CDPR proposal: sCDPR

2.3. Nomenclature

Figure 4 shows the sCDPR proposal in an arbitrary pose to present the nomenclature for the modelling of the robot.

The dimensional parameters, coloured in green, are: W and H, the width and height of the frame, w and h, the width and height of the end-effector, a is the distance between the centre of mass of the end-effector and the centre of the driven pulley located at the top of the end-effector, b the distance between the centre and the bottom of the end-effector, w_{uc} and w_{lc} are the widths of the upper and lower passive carriages, r_t is the radius of the driver pulleys and, r the radius of the driven pulleys attached to the actuators.

The angles of the cables, in red, are α, β and γ which represent the angle with regards to Y axis of the lower inner, upper inner and outer path of the cable loop, respectively.

Being T the pretension of the cable loop, the instant tension of each path of cable loop has been noted as T, $T - \Delta T$ and $T + \Delta T$, and depend on the actuation of the motors attached to the driven pulleys.

The generalised coordinates to develop the model are: q_1, the horizontal coordinate of the end-effector, q_2 the angle with regards to Y axis of the end-effector, q_3 the horizontal coordinate of the lower carriage and q_4 the horizontal coordinate of the upper carriage.

Finally, the input torque of both actuators have been noted as τ_1 and τ_2.

Preprints (www.preprints.org) | NOT PEER-REVIEWED | Posted: 11 April 2023 doi:10.20944/preprints202304.0184.v1

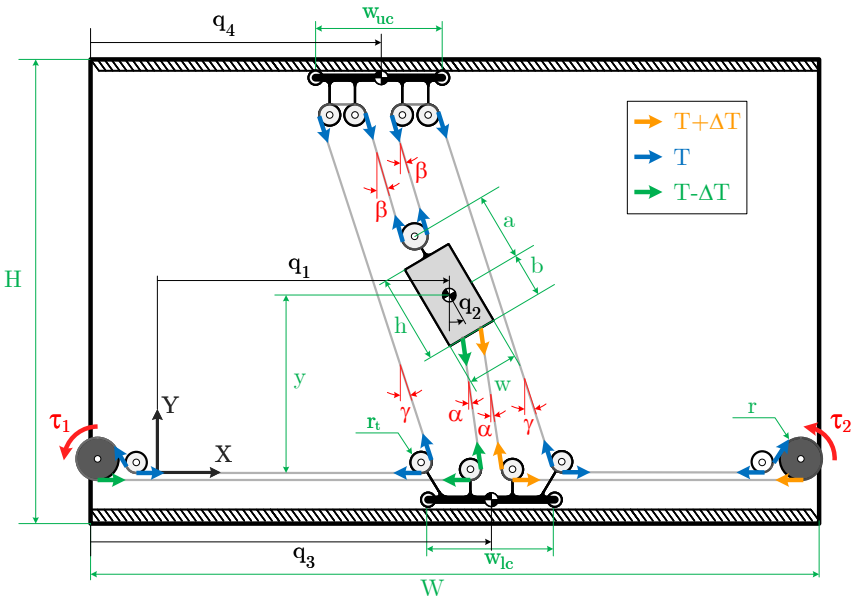

Figure 4. Nomenclature of sCDPR

2.4. Workspace gain

With this novel proposal, assuming that after a movement both carriages are almost aligned to the end-effector in the horizontal axis (see the pose of Figure 3 as example), the equilibrium of forces/torque is guaranteed and the end-effector is therefore able to reach almost all the frame area. In particular, the feasible workspace at static conditions is defined by all end-effector coordinates $[x, y]$ which satisfy:

$$\begin{array}{lll} \frac{w_{lc}}{2} & \leq x \leq & W - \frac{w_{lc}}{2} \\ b & \leq y \leq & H - a \end{array} \tag{1}$$

In the proposal, with a single closed loop of cable, the workspace only depends on the geometry of the frame and the end-effector (see expression (1)). Figure 5 represents the static workspace of the sCDPR proposal for the same parameters of the results regarding to the conventional scheme (see Figure 2).

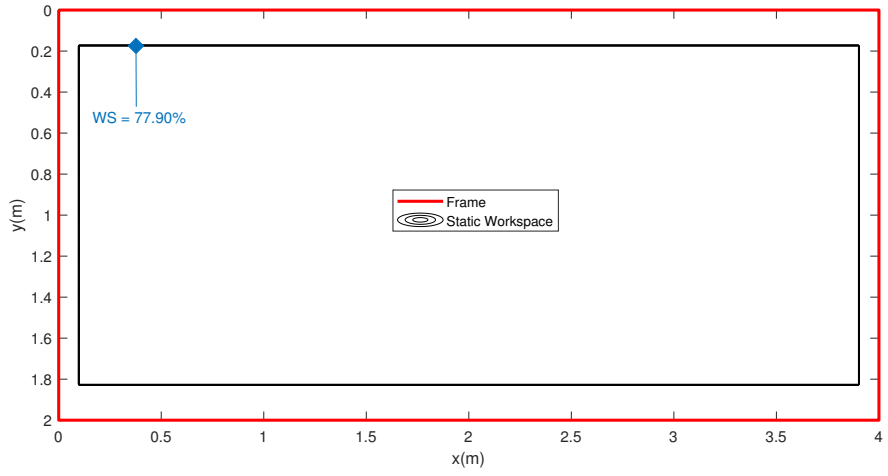

Figure 5. Workspace of the sCDPR

Preprints (www.preprints.org) | NOT PEER-REVIEWED | Posted: 11 April 2023 doi:10.20944/preprints202304.0184.v1

3. Mathematical Model

In this section the mathematical foundations of the new CDPR design are introduced, including the kinematic, static and dynamic models.

3.1. Kinematic Model

In the novel design the kinematic model is much more simple than the one of a conventional CDPR. Owning to the fact that there are only two actuators and one single cable loop, the kinematic model must only take into account the variation of end-effector pose with regards to the angle that the actuators roll up or out the cable. In this sense, the forward kinematic transform yields:

$$[\Delta x_e, \Delta y_e] = \phi^{FK}(\Delta\alpha_1, \Delta\alpha_2), \tag{2}$$

being $\phi^{FK} = [\frac{r(\Delta\alpha_1+\Delta\alpha_2)}{2}, \frac{r(\Delta\alpha_1-\Delta\alpha_2)}{2}]$.

The inverse kinematic transform, on the other hand, can be written as:

$$[\Delta\alpha_1, \Delta\alpha_2] = \phi^{IK}(\Delta x_e, \Delta y_e), \tag{3}$$

being $\phi^{IK} = [\frac{(\Delta x_e-\Delta y_e)}{r}, \frac{(\Delta x_e+\Delta y_e)}{r}]$. It is remarkable how both kinematics only depend on the variation of end-effector position, $\Delta x_e, \Delta y_e$, or angular position of the actuators, $\Delta\alpha_1, \Delta\alpha_2$, and the effective radius of the actuator pulleys, r. As can be seen, the tension or pretension of the cables does not influence the kinematics, but it does influence the positioning accuracy of the end-effector. This issue is addressed in the Dynamic Model Section 3.2, where the influence of the pretension given to the model is noticeable.

On the other hand, when talking of the static model, as mentioned above, the equilibrium of forces is guaranteed. In this sense, it is not necessary to solve a static equilibrium system in order to choose the tension values that remain within the tensions limits while complying with the kinetostatic equilibrium.

Finally, it is important to mention that a notable advantage of the novel proposal is its kinetostatic simplicity (see (2) and (3)).

3.2. Dynamic Model

The dynamic model has been developed under the assumption that angles α, β and γ (see Figure 4) are small enough to obtain a linear equivalent model. In this way, angles of cables can be originally written as:

$$\begin{aligned} \alpha &= \tan^{-1}\left(\frac{q_3-q_1-a\sin(q_2)}{y-a\cos(q_2)}\right) \\ \beta &= \tan^{-1}\left(\frac{q_1-q_4-b\sin(q_2)}{H-y-b\cos(q_2)}\right) \\ \gamma &= \tan^{-1}\left(\frac{q_3-q_4}{H}\right) \end{aligned} \tag{4}$$

The dynamics equations of the actuators and carriages have been obtained by writing their Newtonian balances due to their simplicity. For the pose detailed in Figure 4 the torque equilibrium of the motors yields:

$$\begin{aligned} \tau_1 + r(T-\Delta T) - rT = 0 \\ \tau_2 - r(T+\Delta T) + rT = 0 \end{aligned} \tag{5}$$

In this sense, the instant increment of the tension of the cable loop can be written as:

$$\Delta T = \frac{\tau_1+\tau_2}{2R} \tag{6}$$

The horizontal equilibrium of the lower carriage force is:

Preprints (www.preprints.org) | NOT PEER-REVIEWED | Posted: 11 April 2023 doi:10.20944/preprints202304.0184.v1

$$-m_3\ddot{q_3} + \frac{1}{R}(\tau_1 + \tau_2) - 2T\left[\sin(\gamma) + \sin(\alpha)\right] - 2T\mu\left[\cos(\gamma)\frac{\dot{q_3}}{\dot{q_3}} + \cos(\alpha)\frac{\dot{q_3}}{\dot{q_3}}\right] = 0 \tag{7}$$

and the horizontal equilibrium of the upper carriage is:

$$-m_4\ddot{q_4} + 2T\left[\sin(\gamma) + \sin(\beta)\right] - 2T\mu\left[\cos(\gamma)\frac{\dot{q_4}}{\dot{q_4}} + \cos(\beta)\frac{\dot{q_4}}{\dot{q_4}}\right] = 0 \tag{8}$$

For obtaining the dynamic behaviour of the end-effector Lagrange formulation has been applied, being the Lagrangian, L:

$$L = \frac{1}{2}m_e(\dot{q}_1)^2 + \frac{1}{2}I_e(\dot{q}_2)^2 \tag{9}$$

the equations that describe the dynamics of the end-effector are:

$$\begin{array}{rcl} \frac{d}{dt}\left(\frac{\partial L}{\partial \dot{q}_1}\right) + \frac{\partial L}{\partial q_1} & = & Q_1 \\ \frac{d}{dt}\left(\frac{\partial L}{\partial \dot{q}_2}\right) + \frac{\partial L}{\partial q_2} & = & Q_2 \end{array} \tag{10}$$

where Q_1 is the generalised horizontal force and Q_2 the generalised torque. Assuming that:

$$dW_t = Q_1 dq_1 + Q_2 dq_2 \tag{11}$$

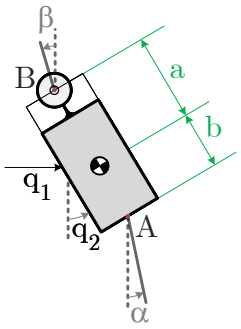

Figure 6. End-effector scheme

being W_t the total work exerted by Q_1 and Q_2. If dW_t is determined Q_1 and Q_2 can be therefore obtained. Assuming the end-effector scheme of Figure 6 dW_t can be determined with by computing the work exerted at points A and B as:

$$dW_t = dW_A + dW_B \tag{12}$$

being $dW_A = \mathbf{F}_A d\mathbf{r}_A$ and $dW_B = \mathbf{F}_B d\mathbf{r}_B$. The A and B differential position arrays can be written as:

$$\begin{array}{rcl} d\mathbf{r}_A & = & [dq_1 + a\cos(q_2)dq_2, \quad a\sin(q_2)dq_2] \\ d\mathbf{r}_B & = & [dq_1 + b\cos(q_2)dq_2, \quad -b\sin(q_2)dq_2] \end{array} \tag{13}$$

and the Forces applied at A and B points as:

$$\begin{array}{rcl} \mathbf{F}_A & = & [\quad 2T\sin(\alpha), \quad -2T\cos(\alpha)] \\ \mathbf{F}_B & = & [\quad -2T\sin(\beta), \quad 2T\cos(\beta)] \end{array} \tag{14}$$

The differential of the total work can be easily obtaining by substituting (13) and (14) in (12):

Preprints (www.preprints.org) | NOT PEER-REVIEWED | Posted: 11 April 2023 doi:10.20944/preprints202304.0184.v1

$$\begin{aligned} dW_t &= 2T[\sin(\alpha) + dq_1 + a\sin(\alpha)\cos(q_2)dq_2 - a\cos(\alpha)\sin(q_2)dq_2] + \\ & \quad 2T[-\sin(\beta)dq_1 + b\sin(\beta)\cos(q_2)dq_2 - b\cos(\beta)\sin(q_2)dq_2] \end{aligned} \tag{15}$$

Identifying (11) with (15), Q_1 and Q_2 can be finally determined:

$$\begin{aligned} Q_1 &= 2T(\sin(\alpha) - \sin(\beta)) \\ Q_2 &= 2T[a(\sin(\alpha)\cos(q_2) - \cos(\alpha)\sin(q_2)) + b(\sin(\beta)\cos(q_2) - \cos(\beta)\sin(q_2))] \end{aligned} \tag{16}$$

$$\begin{aligned} Q_1 &= 2T(\sin(\alpha) - \sin(\beta)) \\ Q_2 &= 2T(a\sin(\alpha - q_2) + b\sin(\beta - q_2)) \end{aligned} \tag{17}$$

By assuming small values of q_2 and that the horizontal distance between both carriages is much smaller than the vertical distance, i.e. $q_3 - q_1 << Y$, $q_4 - q_1 << H - Y$ and $q_3 - q_4 << H$, angles in (4) can be assumed to be:

$$\begin{aligned} \alpha &\approx \tfrac{q_3 - q_1 - a\sin(q_2)}{y - a\cos(q_2)} \\ \beta &\approx \tfrac{q_1 - q_4 - b\sin(q_2)}{H - y - b\cos(q_2)} \\ \gamma &\approx \tfrac{q_3 - q_4}{H} \end{aligned} \tag{18}$$

In this way, developing expressions (10) a linear and time invariant (LTI) dynamic model is finally achieved and expressed as:

$$\mathbf{M}\ddot{\mathbf{q}}(t) + \mathbf{K}\mathbf{q}(t) = \mathbf{w} \tag{19}$$

being $\mathbf{M}$, the mass/inertia matrix:

$$\mathbf{M} = \begin{pmatrix} m_e & 0 & 0 & 0 \\ 0 & I_e & 0 & 0 \\ 0 & 0 & m_3 & 0 \\ 0 & 0 & 0 & m_4 \end{pmatrix} \tag{20}$$

$\mathbf{K}$ the stiffness matrix:

$$\mathbf{K} = \begin{pmatrix} 2T\left(\frac{1}{z_2} + \frac{1}{z_1}\right) & 2T\left(\frac{a}{z_2} - \frac{b}{z_1}\right) & -\frac{2T}{z_2} & -\frac{2T}{z_1} \\ 2T\left(\frac{1}{z_2} - \frac{1}{z_1}\right) & 2T\left(\frac{a^2}{z_2} + a + \frac{b^2}{z_1 b} + b\right) & -\frac{2Ta}{z_2} & \frac{2Tb}{z_1} \\ -\frac{2T}{z_2} & -\frac{2Ta}{z_2} & 2T\left(\frac{1}{H} + \frac{1}{z_2}\right) & -\frac{2T}{H} \\ -\frac{2T}{z_1} & \frac{2Tb}{z_1} & -\frac{2T}{H} & 2T\left(\frac{1}{H} + \frac{1}{z_1}\right) \end{pmatrix} \tag{21}$$

with $z_1 = H - Y - b$, $z_2 = Y - a$ and $\mathbf{w}$ the external force array:

$$\mathbf{w} = \begin{pmatrix} 0 \\ 0 \\ \frac{1}{R}(\tau_1 + \tau_2) - 4T\mu\frac{\dot{q_3}}{\dot{q_e}} \\ -4T\mu\frac{\dot{q_4}}{\dot{q_4}} \end{pmatrix} \tag{22}$$

Dynamic model (19) is valid as long as the small cable angles assumption is fulfilled. Simulation and experimental results will demonstrate the validity of the proposed LTI model for describing the dynamics of the sCDPR.

Preprints (www.preprints.org) | NOT PEER-REVIEWED | Posted: 11 April 2023 doi:10.20944/preprints202304.0184.v1

4. Experimental Platform Description

4.1. Robot description

The experimental platform has been designed to be mainly built by laser cutting and 3D printed parts. Figure 7 shows the designing and the final prototype, including the main functional elements.

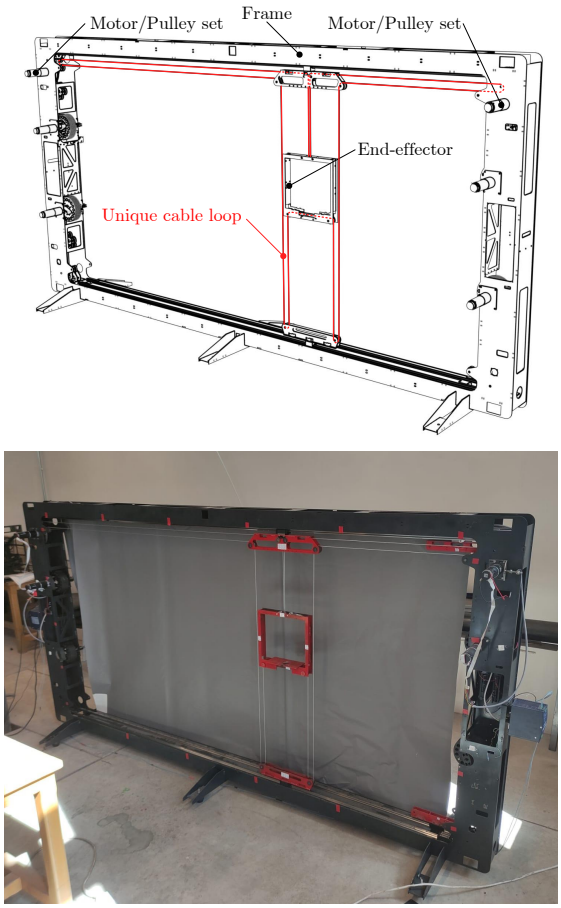

Figure 7. Design and Prototype of the proposed sCDPR

The frame and end-effector are made of 4 mm steel plates cut by laser. The pulleys have been printed with compound material and the cable is a 2 mm of diameter steel cable. The actuators are two DC motors MaxonMotor RE40, with a 26:1 gearbox. They also included 256 ppv encoders to acquire their angular position. The motors are commanded by two servoamplifiers, ESCON 70/10 which receive the control signal from the control device: a NI MyRio 1900 real-time controller. This configuration ensures a sampling frequency of 1 KHz. The cable of the closed loop is a 2 mm of diameter steel cable. Table 1 summarises the main parameters of the robot.

Preprints (www.preprints.org) | NOT PEER-REVIEWED | Posted: 11 April 2023 doi:10.20944/preprints202304.0184.v1

Table 1. Parameters of the prototype

Frame	
Width, W (mm)	2224
Height, H (mm)	1112
End-effector	
Width, w (mm)	287
Height, h (mm)	281
Mass, m_e (Kg)	2.1
Rotational Inertia, I_e (Kg $\cdot$ m ^{2})	$2.5198 \cdot 10^{-2}$
Cable	
Diameter, d (mm)	2
Young's module, E (GPa)	2.0912
Passive Carriages	
Width, $w_3 = w_4$ (mm)	287
Mass, $m_3 = m_4$ (Kg)	1.2
Motor/Pulley sets	
Rotational Inertia, J (Kg $\cdot$ m ^{2})	$1.2734 \cdot 10^{-2}$
Viscous friction coefficient, b (Nms)	0.2
Effective radius, r (mm)	7.3

4.2. Computer vision system

In front of the robot a vision system is placed to track some points of interest during the robot manoeuvres. Four markers have been attached to the frame, four to the end-effector and one at each passive carriage.

The camera is a 8 Megapixels 3264 $\times$ 2448 resolution with a Sony IMX179 sensor. The focal distance, brightness can be manually adjusted. After the camera calibration, the 30fps images are undistorted and the equivalence between images coordinates and world coordinates is obtained. The different points of interest are obtained by a simple colour segmentation, and the position of the end-effector and passive carriages can be therefore obtained after the experiments in an offline way.

Figure 8 represents as example a region of interest of the original image, the marker pose detection by segmentation and the end-effector position estimation.

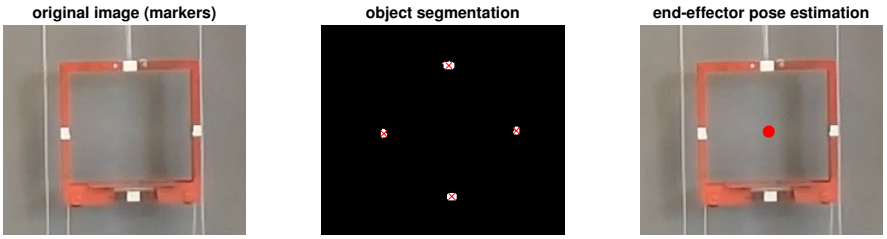

Figure 8. Vision system for pose estimation

5. Model identification and validation

5.1. Parameters identification

The objective of this section is to validate the dynamic model developed in Section 3.2. Dimensional parameters (see Table 1) can be directly measured but the coefficient of friction, μ, shall be identified.

For this purpose, some experiments have been carried out. For a given cable loop pretension value ($T = 350$ N), the voltage which control the servoamplifier has been increased in 0.1 V steps, observing the first voltage value at carriages (and end-effector) start moving. By repeating 30 times the experiment, the average value of voltage is $V_f = 0.68$ V which corresponds to a motor torque of $\tau_f = 0.8826$ Nm.

Preprints (www.preprints.org) | NOT PEER-REVIEWED | Posted: 11 April 2023 doi:10.20944/preprints202304.0184.v1

On the other hand, the dynamic model (19) has been implemented in Matlab®/Simulink® and both motors have been excited with $\tau_f = 0.8826$ N. Changing the value of μ, the one which minimise the error between the experimental and simulated results has been selected, $\mu = 0.1723$.

For illustrative purpose Figure 9 compares the first 10 experimental results and the simulated one after identifying μ value. The horizontal position of the upper carriage, q_4, initially placed at $q_4(0) = 0.2$ m, is represented when V_f is applied in both motors.

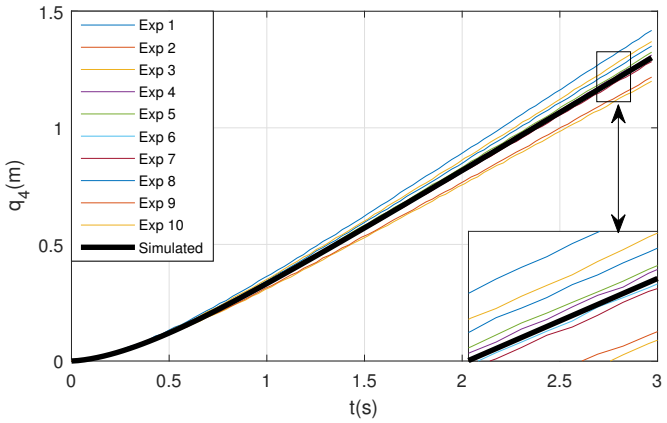

Figure 9. Open loop results: experiments vs. simulation (μ parameter identification)

5.2. Frequency characterisation

In this Section the natural frequency of the robot will be determined to be used in further control strategies to compensate end-effector vibration during the robot manoeuvres. The cable loop pretension value, T, has a notorious influence on this natural frequency. In this way, this frequency has been determined for three values of cable pretension: a low value of 200 N, a medium value of 350 N and a high value of 500 N.

The procedure to determine the natural frequency of the end-effector is the following: For a given end-effector position, an horizontal external force is applied to it; the vision system described in Section 4.2 registers the end-effector pose; its horizontal displacement is therefore acquired, x_e; the continuous frequency component is removed, x_e^0; FFT is applied to determined the maximum frequency peak of the frequency spectrum. Figure 10 illustrates this procedure.

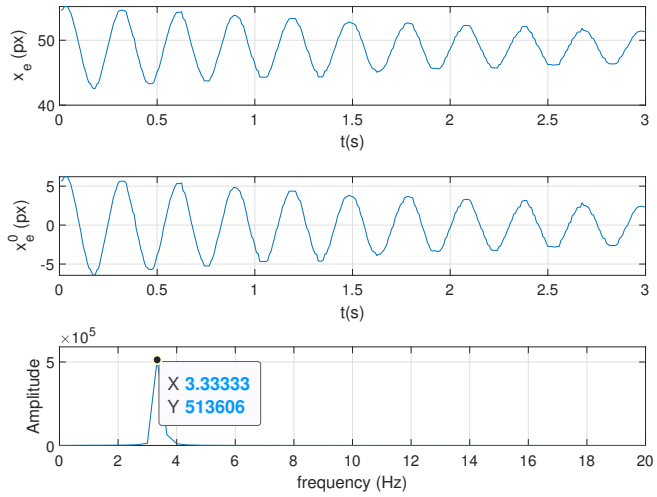

Figure 10. Procedure for natural frequency determination

Preprints (www.preprints.org) | NOT PEER-REVIEWED | Posted: 11 April 2023 doi:10.20944/preprints202304.0184.v1

Figure 11 represents the natural frequency, $f_n(Hz)$, of the end-effector by repeating the aforementioned procedure for different positions (4 position in vertical axis and 5 in horizontal axis).

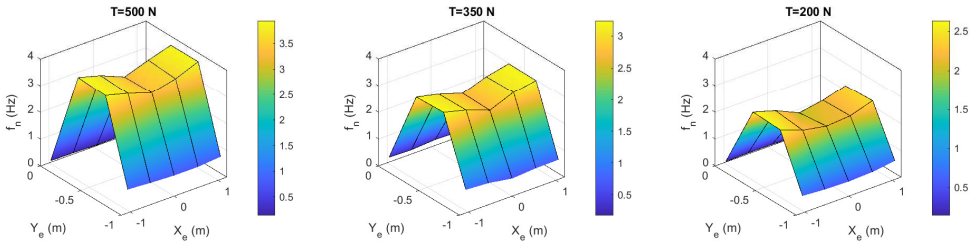

Figure 11. Natural frequency into the robot workspace

Note that natural frequency is low when the end-effector is placed near to the top or to the bottom of the frame and its grow up when vertical position is near of the centre of the frame, where it reached its maximum value. For higher values of cable loop pretension the natural frequency is about 3.9 Hz and for lower values of pretension is about 2.4 Hz.

This frequency characterisation can be used to design a control strategy to remove the non-desirable vibration of the end-effector during its manoeuvres.

5.3. Model validation

Simulated and experimental results are compared in this section for validation purposes. The experiments consist of placing the end-effector in an initial pose and applying a 1 second torque step in both motors. The experiments carried out are summarised in Table 2.

Table 2. Summary of open-loop experiments for validation

Experiment	End-effector position $[x_e, y_e]$ m	Input torques $[\tau_1, \tau_2]$Nm
1	$[0.173, 0.300]$	$[4.85, 4.85]$
2	$[1.830, 0.300]$	$[-4.78, -4.78]$
3	$[0.550, 0.234]$	$[1.87, -1.87]$
4	$[0.550, 0.921]$	$[-1.82, -1.82]$

For all experiments the end-effector position and the carriage positions are compared.

For illustrative purpose, Figure 12 shows the simulated and the experimental results of Experiment 1 in Table 2. In the link here[1] an overlapped video with the simulation and experimental results can be found.

[1] https://www.dropbox.com/s/9reltxle4xujz9t/modelValidation.avi.mp4?dl=0

Preprints (www.preprints.org) | NOT PEER-REVIEWED | Posted: 11 April 2023 doi:10.20944/preprints202304.0184.v1

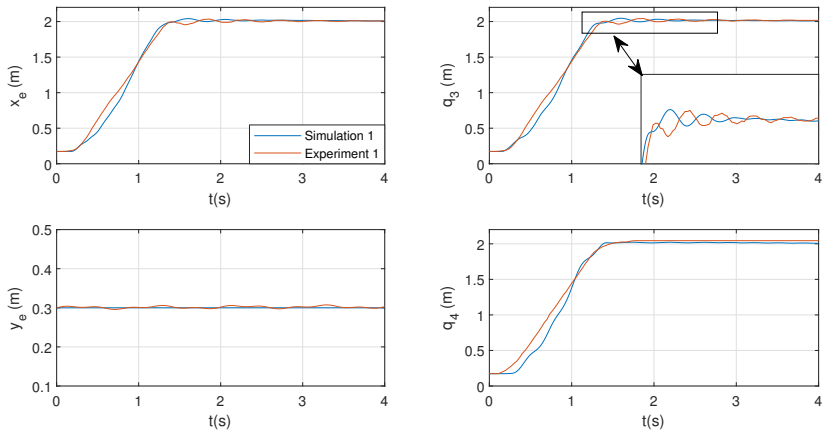

Figure 12. Identification results: experiment 1

In order to validate the small angles assumption in Section 3.2, Figure 13 represents all angles of interest α, β and γ of the model simulation corresponding to experiment 1. Note that during the application of the torque the cable angles reach their maximum value, but it is only about 6° and the small angles assumption for dynamic model can be considered valid.

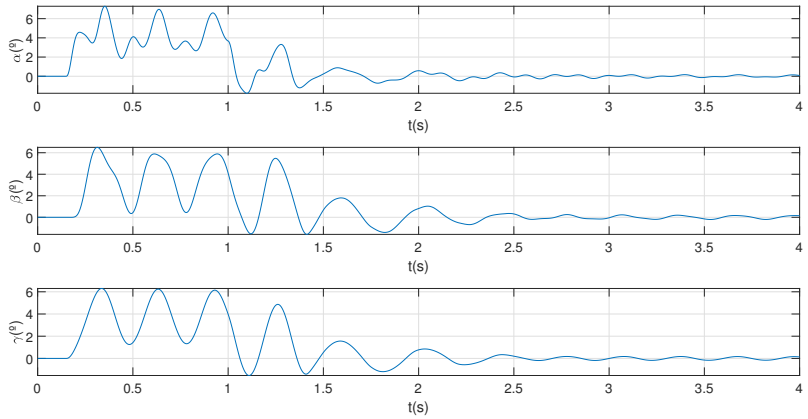

Figure 13. Cables angles in Simulation 1

6. Kinematic control

This section is devoted to show the controlability of the system by means of a simple kinematic control.

6.1. Control scheme

To illustrate the workspace gain of the proposal and the controlability of the system the kinematic control shown in Figure 14 is experimentally implemented. This control scheme assumes that the dynamics of the actuators is decoupled from the sCDPR, i.e. kinematic control is applied as a first approach (e.g. [23]).

In Figure 14 $\mathbf{Q}_e^* = [x_e^*, y_e^*]^T$ is the end-effector position reference, $\boldsymbol{\alpha}^* = [\alpha_1^*, \alpha_2^*]^T$ is the joint coordinates reference, $\boldsymbol{\varepsilon} = [\alpha_1^* - \alpha_1, \alpha_2^* - \alpha_2]^T$ the error signal, $\mathbf{V} = [V_1, V_2]^T$ are the voltage control signal, $\boldsymbol{\tau} = [\tau_1, \tau_2]^T$ the input torque, $\mathbf{Q}_e = [x_e, y_e]^T$ the end-effector pose and $\boldsymbol{\alpha} = [\alpha_1, \alpha_2]^T$ the actual joint coordinates.

Preprints (www.preprints.org) | NOT PEER-REVIEWED | Posted: 11 April 2023 doi:10.20944/preprints202304.0184.v1

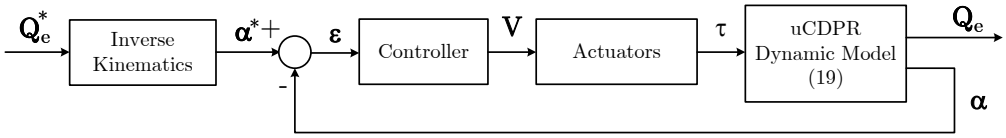

Figure 14. Kinematic control for sCDPR

In this way, as control scheme is based in joint coordinates space, controller block, **R** in Figure 14 is:

$$\mathbf{R} = \begin{bmatrix} R_1 & 0 \\ 0 & R_2 \end{bmatrix} \tag{23}$$

where $R_1 = R_2 = R$ due to mechanical symmetry in the robot design.

To illustrate the controlability of the system a linear PD controller is designed for each actuator set. Its control law can be written as:

$$V_i(t) = K_p \varepsilon_i(t) + K_d \frac{d\varepsilon_i(t)}{dt} \tag{24}$$

for actuator $i = 1, 2$.

The prototype is actuated by means of 2 DC motor/gearbox/driver pulley sets which allow the following transfer function to be identified for the motors:

$$G(s) = \frac{\alpha(s)}{V(s)} = \frac{2169}{s(s + 16.68)} \tag{25}$$

For the frequency requirements, gain crossover frequency, $\omega_c = 40$ rad/s and phase margin, $\varphi_m = 60°$ the resulting controller is;

$$R(s) = 0.6352 + 0.0125s \tag{26}$$

6.2. Position control results

Two simple manoeuvres have been experimentally tested: one horizontal and one vertical. Since the actuators model (25) is of second order, Bezier trajectories of 4^{th} order have been implemented to ensure smooth end-effector trajectories. Both trajectories start at the initial pose of the end-effector, execute a manoeuvre to an intermediate pose, and return to the initial pose.

Table 3 summarises the initial an final end-effector pose and the trajectory time of both controlled manoeuvres.

Table 3. Kinematic control trajectories

Trajectory	Initial pose	Intermediate pose	Final pose	Trajectory time
		$[x_e, y_e]$ m		t_s (s)
Horizontal	$[0.3, 0.55]$	$[1.9, 0.55]$	$[0.3, 0.55]$	4
Vertical	$[0.55, 0.20]$	$[0.55, 0.9]$	$[0.55, 0.20]$	4.5

Figures 15 and 16 represent the reference tracking of the horizontal and vertical trajectories of Table 3. Note that end-effector suffers some vibration during the manoeuvres in coherence with Section 5.2. The objective of this paper is to present the advantages of novel sCDPR scheme and its dynamic model. Control approach presented here will be treated in further works in order to improve the accuracy of the robot by compensating the non-desirable vibration during its movement.

Preprints (www.preprints.org) | NOT PEER-REVIEWED | Posted: 11 April 2023 doi:10.20944/preprints202304.0184.v1

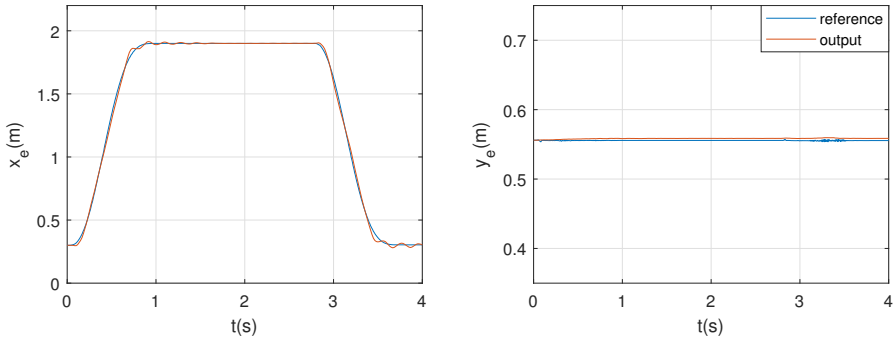

Figure 15. Trajectory tracking: horizontal manoeuvre

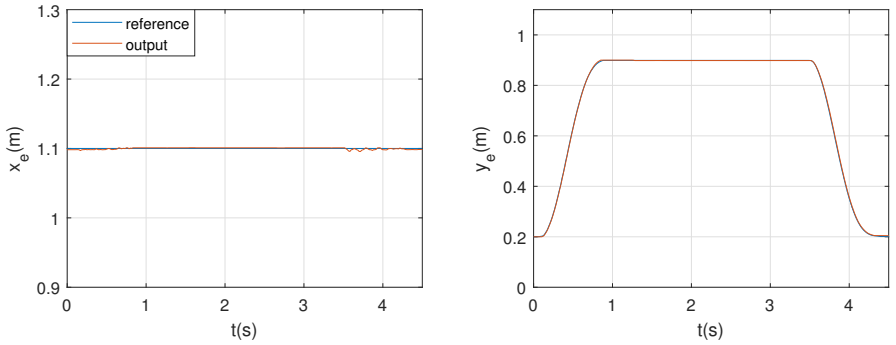

Figure 16. Trajectory tracking: horizontal manoeuvre

Figure 17 represents the euclidean error committed during the trajectories. Note that, although a simple kinematic control has been implemented, for horizontal manoeuvres the maximum error appears during the acceleration and deceleration phase, about 50 mm, and for the vertical about 8 mm.

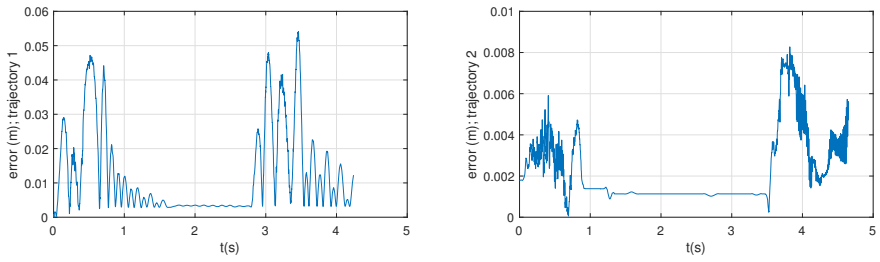

Figure 17. Trajectory tracking error

7. Conclusions

This paper proposes a novel design for planar fully-constrained CDPRs of 3 DOFs. The novelty of the design is based on mechanically modifying the design presented in [18] by using a single cable loop, instead of four different cables.

The novel CDPR includes two passive carriages that move freely along linear guides attached to the robot frame, and a single cable loop driven by two actuators. The end-effector pose is changed by means of a set of driven pulleys while maintaining the cable length constant.

The main goal of the new design is to increase the feasible workspace of the robot in comparison to conventional design. In addition, the stiffness of the robot remains invariant for a given pretension of the cable loop.

After presenting the novel sCDPR scheme, the kinetostatic problem is introduced. One of the advantages of this new design is the simplicity of both, forward and inverse kinematic transforms. The

single cable loop reduces the kinematics to expressions where the variation of pose of the end-effector is directly related to the variation of cable roll in or out by the motors, which are much simpler than the kinematic formulations of the previous CDPR models in [18].

The dynamic model of the system has been also developed bringing a linear and time invariant model which allows to directly apply linear techniques. The dynamic model has been developed under the assumption that end-effector and passive carriages are pseudo-aligned and cables angles are small. Experimental results have been carried out to validate the dynamic model developed.

Finally, a simple kinematic control has been experimentally applied to illustrate the controlability of the system. The kinematic control has been designed considering only the dynamics of the actuators. Experimental results show an acceptable error for the end-effector trajectory tracking.

For removing the residual vibration of the end-effector during horizontal manoeuvres further works will propose more complex control strategy approaches based on the frequency characterisation of the sCDPR.

Author Contributions: Conceptualization, A. González Rodríguez, F.J. Castillo-García and F. Moya-Fernández; methodology, A. Martín-Parra and S. Juárez-Pérez; software, D. Rodríguez Rosa and J. Rosado-Linarez; validation, A. Martín-Parra and F.J. Castillo-García; ; investigation, A. González-Rodríguez and S. Juárez-Pérez; ; writing original draft preparation, A. Martín-Parra, F.J. Castillo-García; supervision, F. Moya-Fernández; project administration, F.J. Castillo-García and A. González-Rodríguez; funding acquisition, F.J. Castillo-García and A. González-Rodríguez. All authors have read and agreed to the published version of the manuscript

Funding: This research was funded by University of Castilla-La Mancha pre-doctoral grant 2020-PREDUCLM-16080 and by Junta de Comunidades de Castilla-La Mancha and European Regional Development Fund grant SBPLY/21/180501/000238

Conflicts of Interest: The authors declare no conflict of interest. The funders had no role in the design of the study; in the collection, analyses, or interpretation of data; in the writing of the manuscript; or in the decision to publish the results

Abbreviations

The following abbreviations are used in this manuscript:

CDPR	Cable-Driven Parallel Robot
sCDPR	Single Cable Cable-Driven Parallel Robot
DOF	Degree-of-freedom
WFW	Wrench-feasible workspace
FFT	Fast Fourier Transform
PD	Proportional-Derivative

References

1. Gouttefarde, M.; Bruckmann, T. Cable-driven parallel robots, 2022.
2. Verhoeven, R. Analysis of the workspace of tendon based Stewart platforms. PhD thesis, Duisburg, Essen, Univ., Diss., 2004, 2006.
3. Tho, T.P.; Thinh, N.T. An Overview of Cable-Driven Parallel Robots: Workspace, Tension Distribution, and Cable Sagging. *Mathematical Problems in Engineering* **2022**, *2022*.
4. Zi, B.; Duan, B.; Du, J.; Bao, H. Dynamic modeling and active control of a cable-suspended parallel robot. *Mechatronics* **2008**, *18*, 1–12.
5. Pott, A. Dynamics. In *Cable-Driven Parallel Robots. Springer Tracts in Advanced Robotics*; Springer International Publishing: Cham, 2018; pp. 229–254.
6. Qian, S.; Zi, B.; Shang, W.W.; Xu, Q.S. A review on cable-driven parallel robots. *Chinese Journal of Mechanical Engineering* **2018**, *31*, 1–11.
7. Pott, A.; Pott, A. Geometric and Static Foundations. *Cable-Driven Parallel Robots: Theory and Application* **2018**, pp. 45–117.
8. Ming, A. Study on multiple degree-of-freedom positioning mechanism using wires (part 1). *Int. J. Japan Soc. Precis. Eng.* **1994**, *28*, 131–138.

9. Lv, W.; Tao, L.; Ji, Z. Sliding mode control of cable-driven redundancy parallel robot with 6 DOF based on cable-length sensor feedback. *Mathematical Problems in Engineering* **2017**, *2017*.
10. Pott, A.; Pott, A. Workspace. *Cable-Driven Parallel Robots: Theory and Application* **2018**, pp. 157–227.
11. Gagliardini, L.; Caro, S.; Gouttefarde, M.; Girin, A. Discrete reconfiguration planning for cable-driven parallel robots. *Mechanism and Machine Theory* **2016**, *100*, 313–337.
12. Youssef, K.; Otis, M.J.D. Reconfigurable fully constrained cable driven parallel mechanism for avoiding interference between cables. *Mechanism and Machine Theory* **2020**, *148*, 103781.
13. An, H.; Yuan, H.; Tang, K.; Xu, W.; Wang, X. A Novel Cable-Driven Parallel Robot With Movable Anchor Points Capable for Obstacle Environments. *IEEE/ASME Transactions on Mechatronics* **2022**, *27*, 5472–5483.
14. Tan, H.; Nurahmi, L.; Pramujati, B.; Caro, S. On the reconfiguration of cable-driven parallel robots with multiple mobile cranes. 2020 5th International Conference on Robotics and Automation Engineering (ICRAE). IEEE, 2020, pp. 126–130.
15. Barbazza, L.; Oscari, F.; Minto, S.; Rosati, G. Trajectory planning of a suspended cable driven parallel robot with reconfigurable end effector. *Robotics and Computer-Integrated Manufacturing* **2017**, *48*, 1–11.
16. Rodriguez-Barroso, A.; Saltaren, R.; Portilla, G.A.; Cely, J.S.; Carpio, M. Cable-driven parallel robot with reconfigurable end effector controlled with a compliant actuator. *Sensors* **2018**, *18*, 2765.
17. Castillo-Garcia, F.J.; Rubio-Gómez, G.; Juárez, S.; Rodríguez-Rosa, D.; Bravo, E.; Ottaviano, E.; Gonzalez-Rodriguez, A. Addition of passive-carriage for increasing workspace of cable robots: automated inspection of surfaces of civil infrastructures. *Smart Structures and Systems, An International Journal* **2021**, *27*, 387–396.
18. Martin-Parra, A.; Juarez-Perez, S.; Gonzalez-Rodriguez, A.; Gonzalez-Rodriguez, A.G.; Lopez-Diaz, A.I.; Rubio-Gomez, G. A novel design for fully constrained planar Cable-Driven Parallel Robots to increase their wrench-feasible workspace. *Mechanism and Machine Theory* **2023**, *180*, 105159.
19. Ottaviano, E.; Arena, A.; Gattulli, V. Geometrically exact three-dimensional modeling of cable-driven parallel manipulators for end-effector positioning. *Mechanism and Machine Theory* **2021**, *155*, 104102.
20. Pott, A. *Cable-Driven Parallel Robots*; Vol. 1, Springer Science & Business Media, 2018.
21. Yuan, H.; Courteille, E.; Deblaise, D. Static and dynamic stiffness analyses of cable-driven parallel robots with non-negligible cable mass and elasticity. *Mechanism and Machine Theory* **2015**, *85*, 64–81.
22. Abdolshah, S.; Zanotto, D.; Rosati, G.; Agrawal, S.K. Optimizing stiffness and dexterity of planar adaptive cable-driven parallel robots. *Journal of Mechanisms and Robotics* **2017**, *9*, 031004.
23. Tang, J.; Zhang, Y.; Huang, F.; Li, J.; Chen, Z.; Song, W.; Zhu, S.; Gu, J. Design and kinematic control of the cable-driven hyper-redundant manipulator for potential underwater applications. *Applied Sciences* **2019**, *9*, 1142.